

Effect of Inlet Downcomer on the Hydrodynamic Parameters of Sieve Trays Using CFD Analysis

Rahbar Rahimi^{*1}, Abolhasan Ameri¹ and Narjes Setoodeh¹

¹ Shahid Nikbakht's Faculty of Engineering, Department of Chemical Engineering, University of Sistan and Baluchestan, Zahedan, Iran

(Received 16 February 2010, Accepted 6 June 2011)

Abstract

Nowadays distillation is recognized as one of the economical and the most trustable separation methods in chemical, petroleum, gas and petrochemical industries. It is almost used as a first and the most applicable choice in separation methods. In this article the effect of inlet downcomer on the hydrodynamics of industrial sieve tray has been elaborated. The study was carried out by using a 3-D Computational Fluid Dynamics (CFD) method and was confirmed with experimental data. Commercial Ansys CFX 11 package software was used for the CFD analysis. Liquid velocity distribution on the tray was in better agreement with experimental data in comparison with simulation results without including inlet downcomer effect. Hydrodynamic parameters of clear liquid height, froth height and average liquid volume fraction in froth were predicted and compared with two available correlations. It was concluded that for having a better simulation model and hence having a deeper insight into tray performance, the downcomer effect on the mass transfer and hydraulic should be considered with CFD analysis.

Keywords: Sieve tray, Hydraulics, Downcomer, CFD, Distillation

Introduction

Distillation is an energy-intensive separation process which is of major importance in the chemical industries and is the first choice for separation of liquid mixtures. Distillation is a process of physically separating a mixture into two or more products that have different boiling points, by preferentially boiling the more volatile components out of the mixture. Sieve trays are widely used in distillation, absorption and liquid-liquid extraction columns in chemical, petroleum and gas industries due to their versatility and low cost. It has been long established that the prediction of distillation tray hydraulics is necessary for indication of separation efficiency and overall tray performance. It is also known that efficiency depends on many involved interrelated parameters, one of which is the flow pattern of liquid on the tray.

Liquid falls through the downcomers by gravity from one tray to the one below it. Downcomers play an important role in separation and hydrodynamic behavior of trays as to some extent, mass transfer occurs in downcomer as well as on the tray deck.

Thus it is significant to focus on the simulation systems considering tray hydrodynamics in the presence of downcomers. Inlet downcomer conditions affect the froth height on the bulk of the tray as well as downstream conditions near exit weir and the crest over it. As liquid flows through the downcomer clearance to the tray deck, a transition from a single phase to two phases flow occurs which makes analysis in the region of the liquid entry quite difficult [1].

A great effort has been done to simulate and model flow maldistributions in order to predict tray efficiencies. The articles on flow patterns in trays by Alexandrov and Vybornov [2], on residence times by Bell [3] and on the effect of channeling on efficiency by Porter *et al.* [4] have appeared followed by similar attempts by Bruin and Freije [5], Bell and Solari [6], Lockett and Safekourdi [7], Sohlo and Kinnunen [8], Solari *et al.* [9], Lockett and Ahmed [10], Solari and Bell [11] and Arreaza [12]. Recently, there have been some attempts to model tray hydrodynamics using CFD. Mehta *et al.* [13] predicted liquid velocity distributions by

considering only liquid phase behavior. Fischer and Quarini [14] presented a 3-D transient model for vapor-liquid hydrodynamics; they assumed a constant value of 0.44 for drag coefficient. Yu *et al.* [15] made an attempt to model the two-phase flow behavior using a two-dimensional model, by focusing on the description of the hydrodynamics along the liquid flow path, while ignoring the variations in the direction of gas flow along the height of the dispersion. Liu *et al.* [16] used a two-dimensional model for simulating the liquid flow pattern. However, the variation of gas flow direction along the dispersion height was ignored. Krishna *et al.* [17] and Baten and Krishna [18, 19] developed CFD models to simulate the transient, three-dimensional two-phase flow behavior of sieve tray for a rectangular and circular geometry, respectively. The required interphase momentum exchange coefficient was estimated on the basis of the correlation of Bennett *et al.* [20] for the liquid holdup. Gesit *et al.* [21] developed a 3-D CFD model to predict the flow patterns and hydraulics of commercial-scale sieve trays. They only considered the outlet downcomer in their modeling. Wang *et al.* [22] used a 3-D pseudo-single-phase CFD model for liquid-phase velocity and concentration distribution on a distillation column tray and estimated an overall efficiency of a 10-tray column. Rahimi *et al.* [23] developed a CFD model to simulate hydrodynamic, temperature and concentration distributions of both liquid and vapor phases and determined the point and tray efficiencies of a sieve tray.

Above mentioned articles assumed that the liquid flowing onto the tray has flat or parabolic profile and have ignored the effect of inlet downcomer. However, by considering the inlet downcomer in the simulations, the assumption of flat or parabolic flow out of downcomer clearance to the tray vanishes and the situation on the tray becomes closer to the actual state.

In this paper a three-dimensional two-phase CFD model is developed to predict the tray hydrodynamics parameters in the

presence of inlet downcomer. The complete geometry including sieve tray, inlet and outlet downcomers were modeled based on the experimental work of Solari and Bell [11] for air-water system. Liquid velocity distribution, clear liquid height, average liquid volume fraction in froth and froth height were predicted using CFD. In other words, the main purpose of this paper is to investigate the extent of the effect of inlet downcomer on sieve tray hydrodynamics.

Model Equations

The dispersed gas and the continuous liquid were modeled in the Eulerian-Eulerian frame work as two interpenetrating phases having separate transport equations. Thus, for each phase the time and volume averaged conservation equations were numerically solved. The energy and mass transfer have not been considered in this work. The two phase conservation equations are as follows.

Continuity Equations

- Gas phase

$$\frac{\partial(r_G \rho_G)}{\partial t} + \nabla \cdot (r_G \rho_G V_G) = 0 \quad (1)$$

- Liquid phase

$$\frac{\partial(r_L \rho_L)}{\partial t} + \nabla \cdot (r_L \rho_L V_L) = 0 \quad (2)$$

Where r , ρ , and V are volume fraction, density and velocity vector, respectively.

Momentum Equations

- Gas phase

$$\begin{aligned} \frac{\partial}{\partial t} (r_G \rho_G V_G) + \nabla \cdot (r_G (\rho_G V_G V_G)) = \\ - r_G \nabla P_G + r_G \rho_G g \\ + \nabla \cdot (r_G \mu_{eff,G} (\nabla V_G + (\nabla V_G)^T)) - M_{GL} \end{aligned} \quad (3)$$

- Liquid phase

$$\begin{aligned} \frac{\partial}{\partial t}(r_L \rho_L V_L) + \nabla \cdot (r_L (\rho_L V_L V_L)) = \\ - r_L \nabla P_L + r_L \rho_L g \\ + \nabla \cdot (r_L \mu_{eff,L} (\nabla V_L + (\nabla V_L)^T)) - M_{GL} \end{aligned} \quad (4)$$

Where the first term at the right hand side of the Eqs. (3) and (4) is indicator of pressure force, the second term is related to gravity and the third term is viscosity term. The term M_{GL} in the momentum equations, represents interphase momentum transfer between the two phases.

Volume Conservation and Pressure Equations

The gas and liquid volume fractions, r_G and r_L , were related by the summation constraint.

$$r_G + r_L = 1 \quad (5)$$

The same pressure field has been assumed for both phases, that is,

$$P_G = P_L = P \quad (6)$$

The effective viscosities of the gas and the liquid phases are $\mu_{eff,G}$ and $\mu_{eff,L}$, respectively.

$$\mu_{eff,G} = \mu_{laminar,G} + \mu_{turbulent,G} \quad (7)$$

$$\mu_{eff,L} = \mu_{laminar,L} + \mu_{turbulent,L} \quad (8)$$

Closure Models

The interphase momentum transfer term, M_{GL} in Eqs. (3) and (4) was given by [17]:

$$M_{GL} = \frac{3}{4} \frac{C_D}{d_G} r_G \rho_L |V_G - V_L| (V_G - V_L) \quad (9)$$

Where d_G is mean bubble diameter and C_D is drag coefficient.

The drag coefficient value (C_D) for the case of distillation is not well known. Fisher and Quarini [14] assumed a constant value of 0.44. This value is appropriate for large bubbles of spherical cap shape. But for the froth flow regime, which is the dominant flow regime in distillation, it is not applicable. Krishna *et al.* [24] have used an equation for drag term that is developed

from their studies on the bubble column. In this study, the drag coefficient, C_D , has been estimated, using the drag correlation of Krishna *et al.* [24], which is a relation, proposed for the rise of a swarm of large bubbles in the Churn-turbulent regime.

$$C_D = \frac{4}{3} \frac{\rho_L - \rho_G}{\rho_L} g d_G \frac{1}{V_{slip}^2} \quad (10)$$

Where the slip velocity, $V_{slip} = |V_G - V_L|$, is estimated from the gas superficial velocity V_s and the average gas holdup fraction in the froth region, $r_G^{average}$, as:

$$V_{slip} = \frac{V_s}{r_G^{average}} \quad (11)$$

For average gas holdup fraction in froth $\alpha_L^{average}$, Bennet *et al.* correlation [20] was used as follows:

$$r_G^{average} = 1 - \alpha_L^{average} \quad (12)$$

$$\alpha_L^{average} = \exp \left[-12.55 \left(V_s \sqrt{\frac{\rho_G}{\rho_L - \rho_G}} \right)^{0.91} \right] \quad (13)$$

Where ρ_G and ρ_L are gas and liquid densities.

By substituting and simplification, the interphase momentum transfer becomes:

$$M_{GL} = \frac{(r_G^{average})^2}{(1 - r_G^{average})^2 V_s^2} g (\rho_L - \rho_G) r_G r_L |V_G - V_L| (V_G - V_L) \quad (14)$$

This correlation is independent of bubble diameters, and this is its major preference over other relations. The standard k- ϵ turbulence model was used for simulating turbulence behavior of the liquid phase. The details of this model are given in the CFX11 solution manual [25]. No turbulence model was used for the gas phase.

Commercial Ansys CFX 11.0 package software on eight 2.76 GHz CPU processors as parallel run was used for solving the equations.

Flow Geometry

Model geometry and the fluids used were based on the experimental work of Solari and Bell [11] carried out at the Fractionation Research Inc. for a 1.213 m diameter sieve tray for air-water system. Due to tray symmetry, only half of it was simulated. The computational space was considered as the 0.61 m distance between two successive trays and also inlet and outlet downcomers. The liquid inlet is at the top of the inlet downcomer as it enters from overhead of the top tray outlet weir and exits at the inlet clearance of the below tray at the bottom of the outlet downcomer. Vapor also enters from the tray holes and leaves at the top of the space between two trays. Table 1 presents tray specifications of Solari and Bell's research [11]. Model geometry is shown in Fig. (1).

Table1: Tray Specifications

Tray diameter (m)	1.213
Tray spacing (m)	0.61
Holes diameter (m)	0.0127
Outlet weir height (m)	0.05
Downcomer clearance (m)	0.038
Downcomer area (%)	13 (Total area)
Hole area (%)	5 (over bubbling area)
Pitch, triangular (m)	0.05
Weir length (m)	0.925

In this simulation an actual number of tray holes, 180 holes of 12.7 mm in diameter per half of tray, were used for vapor inlet. The results sensitivity to grid sizes was investigated for different number of unstructured tetrahedral meshes. The grid convergence requires that after a certain grid size the numerical results do not change significantly as grid size is further decreases. Adjacent to the vapor inlet and near the tray deck, finer meshes were used and away from the tray deck, the mesh sizes became larger. The sensitivity of the simulation results to grid size was checked by comparing the results for 23823, 31257, 47743, 52994, 86902, 97312 and 196956 nodes. As it is shown in table 2, by increasing the number of grids, the CFD prediction results for clear liquid height became slightly better. After

the specified number of nodes the results did not have obvious variations. Hence for lowering computational effort, the simulations were carried out with 86902 nodes. The sample of meshes used in simulations is shown in Fig. (2).

Table2: Sensitivity of the clear liquid height results to number of nodes ($Q_L=0.0178 \text{ m}^3/\text{s}$ and $F_s=0.462$)

Number of nodes	Clear liquid height (m)
23823	0.076537
31257	0.074145
47743	0.074019
52994	0.074232
86902	0.074069
97312	0.074071
196956	0.074070

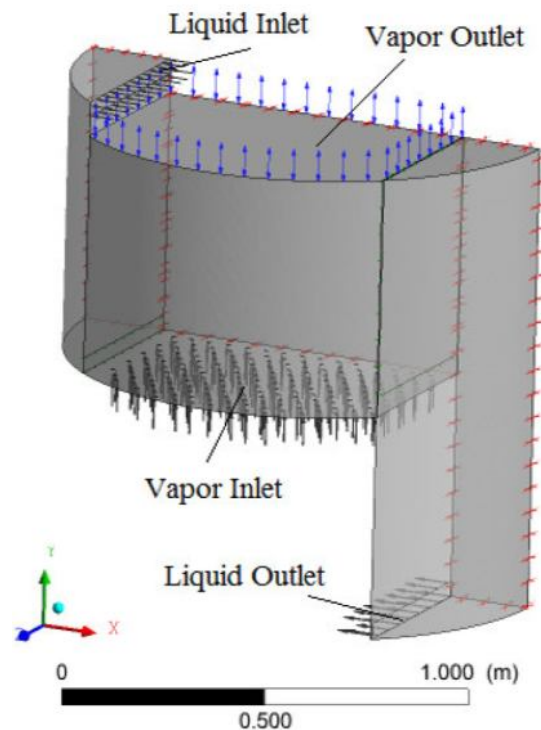


Figure1: Model geometry and boundary conditions

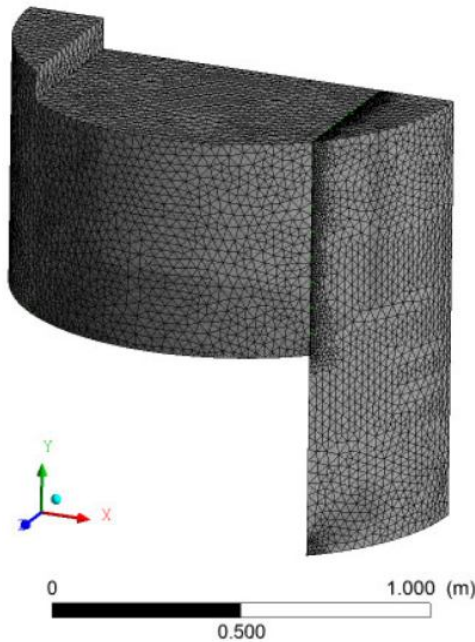


Figure 2: Unstructured mesh of model

Boundary Conditions

In available published works, the velocity profile at the liquid inlet was assumed either flat or parabolic [17-19, 21-23, 26 and 27]. The inlet downcomer has been included in the model simulations to form a more realistic profile and behavior of liquid at the inlet of the tray while eliminating the dependency of liquid flow pattern on the tray to the inlet profile. The liquid volume fraction at the inlet is unity. The boundary condition at the liquid outlet was considered as mass flow. The gas velocity at an inlet hole was calculated as:

$$V_{hole} = \frac{V_s A_B}{\sum_{i=1}^{N_H} A_{hole,i}} \quad (15)$$

At the vapor outlet, pressure boundary condition was specified. At the liquid outlet, only liquid was assumed to leave the flow geometry, similarly, only gas was assumed to exit through the vapor outlet. These specifications were in agreement with the specifications at the gas and liquid inlet, where only one phase was assumed to enter. A no-slip wall boundary condition was specified for the liquid phase and a free slip

wall boundary condition was used for the gas phase. At the plane of symmetry, the normal component of velocity was zero and the gradients of the other variables in the transverse direction were taken to be zero.

Simulation Results and Discussion

The CFD analysis and transient simulations were carried out using the commercial package ANSYS CFX 11. The upwind advection scheme was used for solving all equations. Also for the time term, a fully implicit second order backward time differencing scheme was used with fixed time steps of 1.0×10^{-3} s. Runs continued until quasi-steady state conditions were established, in other words, a simulation was deemed to have converged whenever the clear liquid height value reached a value with no considerable change in successive time steps. Although the simulations were inherently transient, an averaged quantity like the clear-liquid height appeared to have reached a steady value, as seen in Figure (3). Such indicators were used to terminate a simulation, even if local values were changing with time in a bounded, chaotic manner.

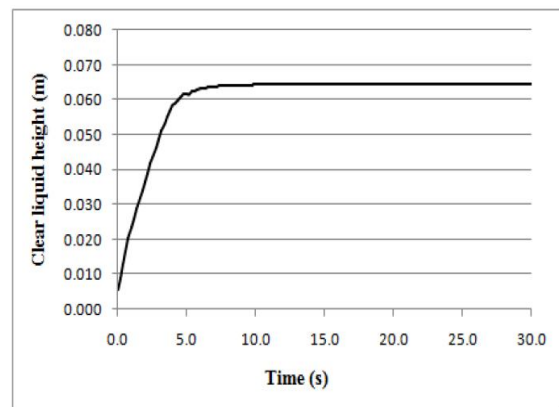


Figure3: Transient simulation convergence as indicated by a plot of clear liquid height vs. time

Velocity Distribution

Solari and Bell [11] in their experimental work estimated the average velocity of the liquid by dividing the distance between two consecutive probes located in the same longitudinal row by the difference in mean residence time between the two probes. The

probes were held about 0.038 m above tray floor. Referring to Figure (4), velocities were determined between the probe line including probes 5, 6, 7, 8 and the probe line consisting probes 9, 10, 11, 12, respectively. Velocities were also measured between the latter one and the probe line 13, 14, 15 and 16, respectively. The first calculation yielded an average velocity distribution in the middle section of the tray (upstream profile); the second one approximated the velocity distribution at the tray outlet (downstream profile) [11]. In our model geometry, probes 5 to 8 lay on $x=0.209$ m and probes 9 to 12 lay on $x=0.438$ m. In order to compare the experimental measurements with the CFD predictions, line integrals of the horizontal component of the liquid velocity were taken on the plane $y=0.038$ m between $x=0.209$ and $x=0.438$ m. The resulting velocity profiles have been referred to as upstream profiles. Similarly, line integrals were taken between $x=0.438$ and $x=0.667$ m for the measurements made between the middle of the tray and the outlet weir, with the resulting velocity profiles designated as downstream profiles.

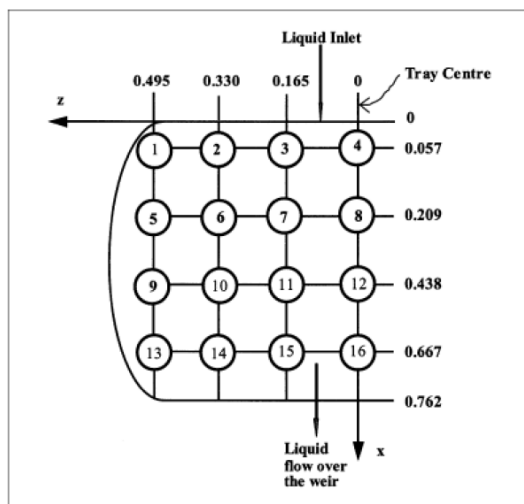


Figure 4: Probe positions on experimental sieve tray of Solari and Bell (1986)

Liquid horizontal velocities predicted by CFD simulations were compared with the experimental data of Solari and Bell [11] and simulation results of Gesit *et al.* [21] at different operating conditions. The

comparisons are shown in Figures (5) to (8). The CFD simulation results are in good agreement with the experimental data of Solari and Bell [11]. In most points, the current simulation results were closer to the experimental data than the simulation results of Gesit *et al.* [21] who excluded the inlet downcomer in their model but assumed a parabolic liquid velocity for the liquid entering the tray. The uncertainties in the specification of this inlet boundary condition (which are often not well characterized in experiments) might be one of the reasons for some of the discrepancies observed between the CFD predictions and the experimental data [21]. So by considering the inlet downcomer into the computational domain, this dependency was eliminated.

Conventional downcomers seen from above are wide in the center, narrowing toward the sides. This shape tends to enhance the liquid flow, down through the center of the downcomer which results in higher liquid velocities along the centerline of the tray, which itself leads to decrease liquid velocity from the tray center toward the tray wall. Non-uniform flow patterns exist on commercial scale sieve trays. These patterns range from simple non-uniform velocity distributions to extensive reverse or retrograde flow near the walls. In the latter case, there is a high speed flow through the center of the tray and a tendency for pooling on either side of the centerline. The pooling results from regions in which the circulation is closed. As seen in Figure (9), a stagnant and recirculation zone was obvious next to the wall side of the tray in the CFD simulation results.

Clear Liquid Height, Froth Height, and Average Liquid Volume Fraction in Froth

As the liquid holdup parameter is used for the prediction of hydraulic parameters such as, pressure drop, average residence time distribution of liquid phase and efficiency, attention have been focused on the variation of liquid holdup of sieve trays.

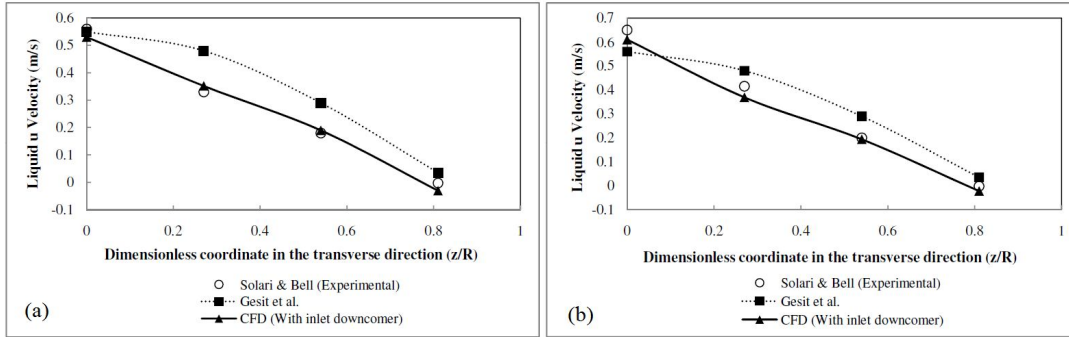


Figure 5: Liquid U velocity profile for $Q_L = 0.0178 \text{ m}^3/\text{s}$ and $F_s = 0.462$
(a)Upstream profile (b) Downstream profile

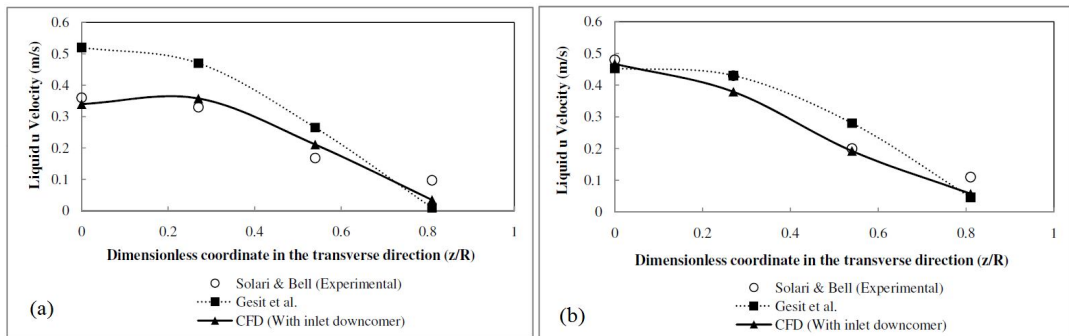


Figure 6: Liquid U velocity profile for $Q_L = 0.0178 \text{ m}^3/\text{s}$ and $F_s = 0.801$
(a)Upstream profile (b)Downstream profile

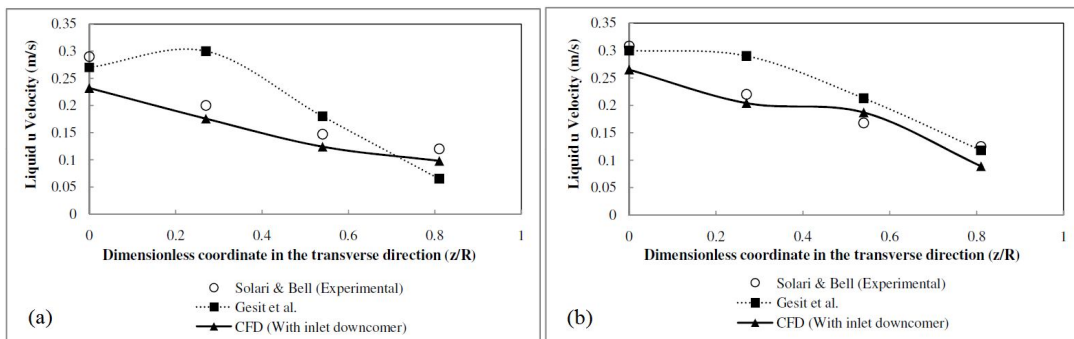


Figure 7: Liquid U velocity profile for $Q_L = 0.00694 \text{ m}^3/\text{s}$ and $F_s = 1.015$
(a)Upstream profile (b)Downstream profile

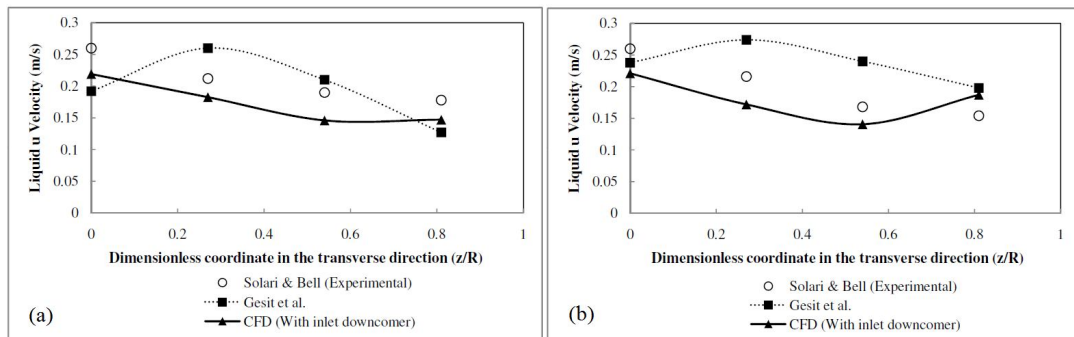


Figure 8: Liquid U velocity profile for $Q_L = 0.00694 \text{ m}^3/\text{s}$ and $F_s = 1.464$
(a)Upstream profile (b)Downstream profile

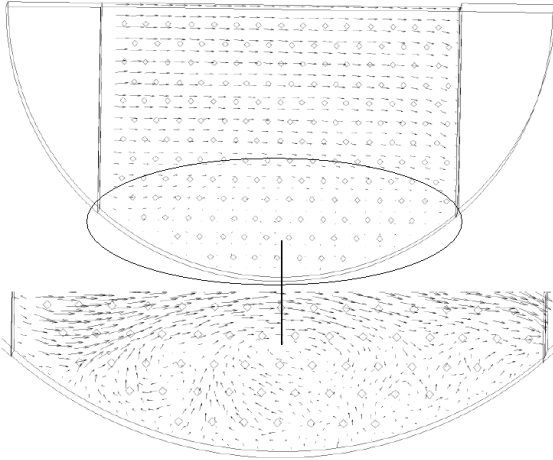


Figure 9: Stagnant and recirculation zone near wall side of the tray

This has led to the calculation of clear liquid height, froth height and liquid holdup fraction in froth. The values of these parameters from the simulations were obtained after averaging over a sufficiently long time interval once quasi-steady state conditions were established. That means the liquid holdup in the system or clear liquid height remained practically constant for the long period of time. Clear-liquid height is defined as the height of liquid that would exist on the tray in the absence of vapor flow. It was calculated as the tray spacing (0.61 m) multiplied by the average volume of the liquid volume fraction above the bubbling area of the tray floor (total computational space minus the space of the two downcomers).

The froth region is usually defined as the region in which the liquid volume fraction is greater than 10%. The average froth height has been calculated as the average area over planes at which the liquid volume fraction is more than 10%.

In sieve tray design, clear liquid height, froth height and average liquid volume fraction in froth are not independent. But CFD has the ability of determining these three parameters independently. Average liquid volume fraction is calculated as the average volume of the liquid volume fraction in froth or the ratio of clear liquid height to froth height.

In our work, CFD simulation results that were obtained for clear liquid height were

compared with the experimental work of Solari and Bell [11], the correlations of Bennett *et al.* [20], Colwell *et al.* [28] and Gesit *et al.* [21] CFD simulation results. The Bennett *et al.* correlation for clear liquid height is [20];

$$h_{cl} = \alpha_L^{average} \left[h_w + C \left(\frac{Q_L}{L_w \alpha_L^{average}} \right)^{0.67} \right] \quad (16)$$

$$C = 0.5 + 0.438 \exp(-137.8 h_w) \quad (17)$$

Where $\alpha_L^{average}$ is average liquid volume fraction in froth and is determined from Equation (13). Colwell *et al.* [28] presented correlations for calculation of clear liquid height and average liquid volume fraction in froth which required trial and error procedure. The set of Colwell *et al.* correlations are given in table 3.

Figure (10) shows clear liquid height for CFD, correlations results at different F_s , as well as Gesit *et al.* results. It showed that with increasing the F-factor, the clear liquid height decreased at constant liquid flow rate.

Table 3. Colwell et al. [28] correlations for calculation of clear liquid height and average liquid volume fraction in froth

Colwell et al. correlations	
$h_{cl} = \alpha_L^{average} \left[h_w + 0.527 \left(\frac{Q_L}{C_D \alpha_L^{average}} \right)^{0.67} \right]$	(18)
$C_D = 0.61 + 0.08 \frac{h_{fow}}{h_w} \quad \frac{h_{fow}}{h_w} < 8.135$	(19)
$C_D = 1.06 \left(1 + \frac{h_w}{h_{fow}} \right)^{1.5} \quad \frac{h_{fow}}{h_w} \geq 8.135$	(20)
$h_{fow} = h_f - h_w$	(21)
$\alpha_L^{average} = \frac{1}{\eta + 1}$	(22)
$\eta = 12.6 Fr'^{0.4} \left(\frac{A_B}{A_h} \right)^{0.25}$	(23)
$Fr' = Fr \left(\frac{\rho_G}{\rho_L - \rho_G} \right)$	(23)

It was increased by increasing liquid flow at constant F-factor as is shown in Figure (11). Like results reported by Gesit *et al.* [21] and

Baten and Krishna [17] our predicted results also gave higher values than experimental values of Solari and Bell [11]; Because the interphase momentum drag term in the Bennet *et al.* [20] correlation ignores coalescence caused by impurities. The noticeable point was that the predicted results were closer to results from Solari and Bell and Bennett *et al.* correlation than the one obtained by Gesit *et al.* without inlet downcomer.

Predicted values of the average liquid volume fraction in froth and froth height compared with correlations recommended for this parameter are shown in Figures (12) and 13. Both curves matched more with the Bennett *et al.* correlation than the Colwell's. Again, these showed the important role of inlet downcomer on simulation results in comparison with Gesit results.

Complete explanation of the cause of difference in the values of these three parameters for two correlations is reported in the literature [21].

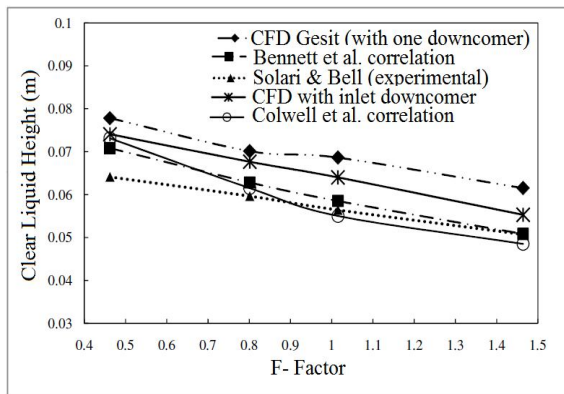


Figure 10: Clear liquid height variation as a function of F-factor (F_s) for constant liquid rate, $Q_L = 0.0178 \text{ m}^3/\text{s}$

In Figure (14), profiles of the liquid volume fraction on a vertical plane of 0.215 m from the tray center are shown at different operating conditions. Due to boundary conditions set and CFD solution, weeping did not occur.

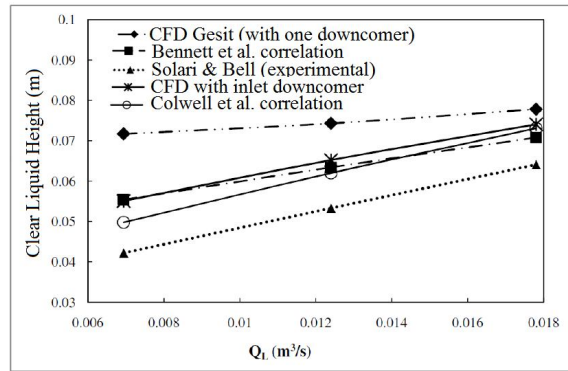


Figure 11: Clear liquid height variation as a function of liquid flow rate (Q_L) for constant F-factor, $F_s = 0.462 \text{ m/s}^2$

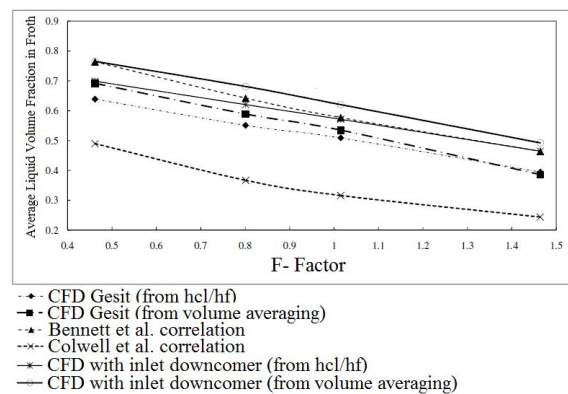


Figure 12: Average liquid volume fraction in froth variation as a function of F-factor (F_s) for constant liquid rate, $Q_L = 0.0178 \text{ m}^3/\text{s}$

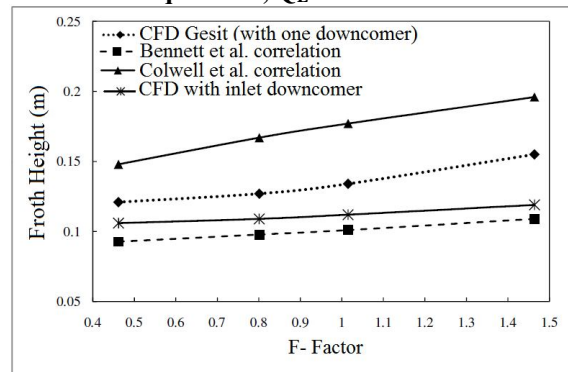


Figure 13: Froth height variation as a function of F-factor (F_s) for constant liquid rate, $Q_L = 0.0178 \text{ m}^3/\text{s}$

As vapor entered through the tray holes, it found a way up through the pool of the liquid on the tray. Around the holes, liquid volume fraction reduced. By increasing the gas rate, expansion of froth height and decreasing of average liquid volume fraction was observed. As liquid flowed to the inlet downcomer, a cascade of free falling liquid

occurred. This caused a circulation in the liquid pool at the bottom of the downcomer. This phenomenon is shown by the vector plot of Figure (15). The liquid level in the downcomer had to overcome the pressure drop for the flow of liquid-vapor mixture to the outlet downcomer. Liquid leveling in the inlet downcomer directs the designer to predict flooding criteria. There was not a liquid level in the outlet boundary; as no resistance was set for liquid outlet boundary.

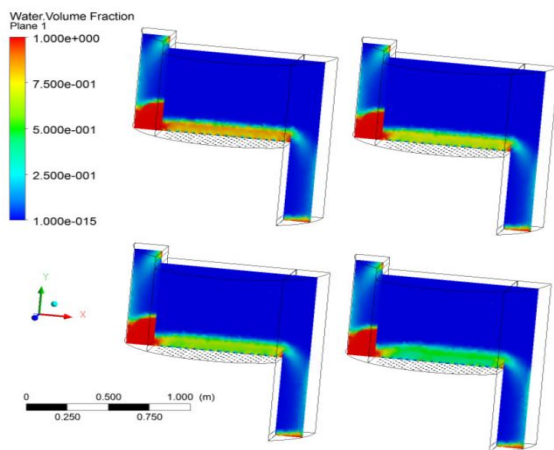


Figure 14: Profiles of liquid volume fraction on a vertical plane; 0.215 m from the tray center at different operating conditions

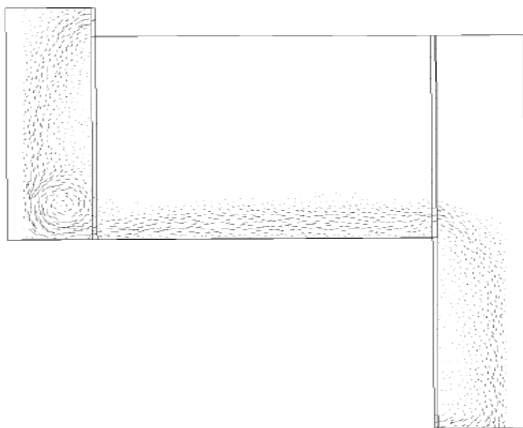


Figure 15: Liquid vector plot on a vertical plane 0.215 m from the tray center

Conclusions

A transient 3-D two-fluid CFD model was developed in the Eulerian-Eulerian framework to predict the hydraulics of sieve trays by considering the inlet downcomer in the simulations. The gas and liquid phase equations were coupled through an

interphase momentum transfer term that was estimated locally, using the drag coefficient correlation of Krishna *et al.* and the liquid holdup fraction correlation of Bennett *et al.* Tray geometry and operating conditions were based on the experimental work of Solari and Bell done at Fractionation Research Inc. (FRI) for a 1.213 m in diameter sieve tray for air-water system. Velocity distribution, clear liquid height, froth height and average liquid holdup in froth were predicted using CFD. The main advantage of this work was studying the effect of inlet downcomer on these parameters. The results showed that for almost all parameters our results were closer to experimental data than Gesit *et al.* results without inlet downcomer. This showed that probably the inlet downcomer has a great effect on mass transfer in distillation and absorption columns. So determining the Murphree and point efficiency from the simulation results based on complete geometry with both downcomers, can lead to better results and more realistic conditions.

This study showed that a virtual experiment can be developed to evaluate the tray performance by means of CFD.

Nomenclature

A_B : tray bubbling area, m^2

A_h : total area of holes, m^2

C_D : drag coefficient

d_G : mean bubble diameter, m

$Fr = \left(\frac{V_s^2}{gh_{cl}}\right)$: froude number

$Fr' = Fr \left(\frac{\rho_G}{\rho_L - \rho_G}\right)$: modified froude number

$F_s = V_s \sqrt{\rho_g}$: F-factor, $m.s^{-2}$

g : gravity acceleration, $m.s^{-2}$

h_{cl} : clear liquid height, m

h_f : froth height, m

h_{fow} : height of froth crest over weir, m

h_w : weir height, m

L_w : weir length, m

M_{GL} : interphase momentum transfer, $kg.m^{-2}.s^{-2}$

P_G : gas- phase pressure, $N.m^{-2}$

P_L : liquid- phase pressure, $N.m^{-2}$
 Q_L : liquid volumetric flow rate, $m^3.s^{-1}$
 r_G : gas- phase volume fraction
 $r_G^{average}$: average gas hold-up fraction in froth
 r_L : liquid- phase volume fraction
 t : time, s
 V_G : gas- phase velocity vector, $m.s^{-1}$
 V_{hole} : gas- phase hole velocity, $m.s^{-1}$
 V_L : liquid- phase velocity vector, $m.s^{-1}$
 V_s : gas- phase superficial velocity based on
 bubbling area, $m.s^{-1}$
 V_{slip} : slip velocity, $m.s^{-1}$

Greek Symbols

$\alpha_L^{average}$: average liquid hold-up fraction in
 froth
 $\mu_{eff.G}$: effective viscosity of gas, $kg.m^{-1}.s^{-1}$
 $\mu_{eff.L}$: effective viscosity of liquid,
 $kg.m^{-1}.s^{-1}$
 ρ_G : gas density, $kg.m^{-3}$
 ρ_L : liquid density, $kg.m^{-3}$

References:

- 1- Lockett, M.J. (1986). *Distillation tray fundamentals*, Cambridge University Press, Cambridge.
- 2- Alexandrov, L.A. and Vybornov, V.G. (1971). "Investigation of the hydrodynamic pattern of liquid flow on crossflow trays." *Tear. Osnovy Kim. Tekn.*, Vol. 5, 339.
- 3- Bell, R.L. (1972). "Experimental determination of residence time on commercial scale distillation trays using fiber optic technique," *AIChE J.*, Vol. 18, PP. 491-497.
- 4- Porter, K.E., Lockett, M.J. and Lim, C.T. (1972). "The effect of liquid channeling on distillation plate efficiency," *Trans. Inst. Chem. Engrs.*, Vol. 50, PP. 91-101.
- 5- Bruin, S. and Freije, A.D. (1974). "A simple mixing model for distillation plates with stagnant zones." *Trans. Inst. Chem. Engrs.*, Vol. 52, PP. 75-79.
- 6- Bell, R.L. and Solari, R.B. (1974). "Effect of nonuniform velocity fields on distillation tray efficiency," *AIChE J.*, Vol. 20, PP. 688-695.
- 7- Lockett, M.J. and Safekourdi, A. (1976). "The effect of the liquid flow pattern on distillation plate efficiency." *Chem. Eng. J.*, Vol. 11, PP. 111-121.
- 8- Sohlo, J. and Kinnunen, S. (1977). "Dispersion and flow phenomena on a sieve plate." *Trans. Inst. Chem. Engrs.*, Vol. 55, PP. 71-73.
- 9- Solari, R.B., Saez, A.E., Apollo, I. D. and Bellet, A. (1982). "Velocity distribution and liquid flow patterns on industrial sieve trays." *Chem. Eng. Commun.*, Vol. 13, PP. 369-384.
- 10- Lockett, M.J. and Ahmed, I.S. (1983). "Tray and point efficiencies from a 0.6 m diameter distillation column." *Chem. Eng. Res. Des.*, Vol. 6, PP. 110-118.
- 11- Solari, R.B. and Bell, R.L., (1986). "Fluid flow patterns and velocity distribution on commercial-scale sieve trays." *AIChE J.*, Vol. 32, PP. 640-649.
- 12- Arreaza, G. (1986). M. Sc. Thesis, Universidad Simon Bolivar.

- 13- Mehta, B., Chuang, K.T. and Nandakumar, K. (1998). "Model for liquid phase flow on sieve trays." *Chem. Eng. Res. Des., Trans.IChemE*, Vol. 76, PP. 843-848.
 - 14- Fischer, C.H. and Quarini, J.L. (1998). "Three-dimensional heterogeneous modeling of distillation tray hydraulics." *AICHE Meeting*, Miami Beach, FL.
 - 15- Yu, K.T., Yuan, X.G., You, X.G. and Liu, C.T. (1999). "Computational fluid-dynamics and experimental verification of two-phase two-dimensional flow on a sieve column tray." *Trans. Inst. Chem. Eng., Part A.*, Vol. 77, PP. 554-560.
 - 16- Liu, C.J., Yuan, X.G., Yu, K.T. and Zhu, X.J. (1999). "A fluid dynamic model for flow pattern on a distillation tray." *Chem. Eng. Sci.*, Vol. 55, PP. 2287-2294.
 - 17- Krishna, R., Van Baten, J.M., Ellenberger, J., Higler, A.P. and Taylor, R. (1999). "CFD simulations of sieve tray hydrodynamics." *Trans.IChemE*, Vol. 77, PP. 639-646.
 - 18- J Van Baten, J.M. and Krishna, R. (2000). "Modeling sieve tray hydraulics using computational fluid dynamics." *Chem.Eng.J.*, Vol. 77, PP. 143-151.
 - 19- Krishna, R. and Van Baten, J.M. (2003). "Modeling sieve tray hydraulics using computational fluid dynamics." *Trans.IChemE.*, Vol. 81, PP. 27-38.
 - 20- Bennett, D.L., Rakesh Agrawal and Cook, P.J. (1983). "New pressure drop correlation for sieve tray distillation columns." *AICHE J.*, Vol. 29, PP. 434-442.
 - 21- Gesit, G., Nandakumar, K. and Chuang, K.T. (2003). "CFD modeling of flow patterns and hydraulics of commercial-scale sieve trays." *AICHE J.*, Vol. 49, PP. 910-924.
 - 22- Wang, X. L., Liu, C. J., Yuan X. G. and Yu, K. T. (2004). "Computational fluid dynamic simulation of three-dimensional liquid flow and mass transfer on distillation column trays." *Ind.Eng.Chem.Res.*, Vol. 43, PP. 2556-2567.
 - 23- Rahimi, R., Rahimi, M.R., Shahraki, F. and Zivdar, M. (2006). "Efficiencies of sieve tray distillation columns by CFD simulations." *Chem. Eng and Technol*, Vol. 29, No. 3, PP. 326-335.
 - 24- Krishna, R., Urseanu, M.I., van Baten, J.M. and Ellenberger, J. (1999). "Rise velocity of a swarm of large gas bubbles in liquids." *Chem. Eng. Sci.*, Vol. 54, PP. 171-183.
 - 25- CFX User Manual, ANSYS, Inc. Modeling, CFX 11.0: Solver.
 - 26- Zarei, T., Rahimi, R. and Zivdar, M. (2009). "Computational fluid dynamic simulation of MVG tray hydraulics." *Korean J. Chem. Eng.*, Vol. 26, PP. 1213-1219.
 - 27- Zarei, A. (2010). Investigation of weeping and entrainment effects on the distillation tray by CFD, M. Sc. Thesis, University of Sistan and Baluchestan, Zahedan, Iran.
 - 28- Colwell, C.J. (1981). "Clear liquid height and froth density on sieve trays." *Ind. Eng. Chem. Proc. Des. Dev.*, Vol. 20, PP. 298-306.
-